Biochimie 94 (2012) 1943–1950

Contents lists available at SciVerse ScienceDirect

Biochimie

journal homepage: www.elsevier.com/locate/biochi

Research paper

Temperature adaptations in psychrophilic, mesophilic and thermophilic chloride-dependent alpha-amylases

Alexandre Cipolla [a], François Delbrassine [a], Jean-Luc Da Lage [b], Georges Feller [a,*]

[a] Laboratory of Biochemistry, Center for Protein Engineering, University of Liège, B-4000 Liège-Sart Tilman, Belgium
[b] UPR9034 Evolution, Génomes et Spéciation, CNRS, F-91198 Gif-sur-Yvette, France and Université Paris-Sud, 91405 Orsay cedex, France

ARTICLE INFO

Article history:
Received 20 March 2012
Accepted 12 May 2012
Available online 23 May 2012

Keywords:
Alpha-amylase
Extremophiles
Antarctic
Differential scanning calorimetry
Protein stability

ABSTRACT

The functional and structural adaptations to temperature have been addressed in homologous chloride-dependent α-amylases from a psychrophilic Antarctic bacterium, the ectothermic fruit fly, the homeothermic pig and from a thermophilic actinomycete. This series covers nearly all temperatures encountered by living organisms. We report a striking continuum in the functional properties of these enzymes coupled to their structural stability and related to the thermal regime of the source organism. In particular, thermal stability recorded by intrinsic fluorescence, circular dichroism and differential scanning calorimetry appears to be a compromise between the requirement for a stable native state and the proper structural dynamics to sustain the function at the environmental/physiological temperatures. The thermodependence of activity, the kinetic parameters, the activations parameters and fluorescence quenching support these activity–stability relationships in the investigated α-amylases.

1. Introduction

Life has successfully colonized nearly all environments on Earth, from the permanently frozen polar regions or the arctic permafrost, to the extremely hot deep-sea hydrothermal vents, hot springs or geysers. The range of temperatures compatible with life is quite large and is currently estimated from −20 °C in sea ice [1] to 122 °C in hydrothermal vents [2]. Microorganisms living in these environments are able to cope with the local chemical and physical extreme parameters by various adaptive strategies in order to maintain activity and metabolic functions despite these challenging conditions [3,4]. From an evolutionary perspective, current views suggest that the last universal common ancestor (LUCA) was mesophilic or moderately thermophilic and that extant extremophiles have subsequently colonized harsh environments [5]. However, there are also arguments for a hot origin of life [6,7] and even for a cold origin [8,9]. It is therefore of interest to understand the molecular mechanisms of adaptation to temperature in contemporary enzymes. In a first step towards this goal, we have compared homologous psychrophilic, mesophilic and thermophilic α-amylases. Temperature adaptation has been well studied in thermophiles [10] while this remains fragmental in psychrophiles [11]. Furthermore, comparisons of homologous series of extremophilic and mesophilic proteins are scare [12–16].

α-Amylases (α-1,4-glucan-4-glucanohydrolase, EC 3.2.1.1) are ubiquitous and widely distributed in microorganisms, plants and animals. These enzymes belong to family 13 in the glycoside hydrolase classification (http://www.cazy.org/and [17]) and catalyze the hydrolysis of internal α(1,4)-glycosidic bonds with net retention of the anomeric configuration in starch, amylose, amylopectin, glycogen and other related polysaccharides through multiple attacks toward the non-reducing ends. As a result of the huge diversity of organisms that synthesize α-amylases, these enzymes exhibit in general a very low degree of sequence similarity, although they adopt the same overall fold [18]. Amongst these enzymes, animal-type α-amylases are homologous enzymes present in all bilaterian animals and in some rare microorganisms, a lateral gene transfer having likely occurred between the two groups [19–22]. All animal-type α-amylases isolated so far display the unusual property to bind a chloride ion at a specific site that induces allosteric activation of the full amylolytic activity. It has been shown that the chloride ion is responsible for the p*Ka* shift of catalytic residues via interactions with active site carboxyl groups [23–25].

Chloride-dependent α-amylases from the Antarctic bacterium *Pseudoalteromonas haloplanktis* and its close homolog from pig

Abbreviations: AHA, α-amylase from *Pseudoalteromonas haloplanktis* (psychrophile); DMA, α-amylase from *Drosophila melanogaster* (ectothermic mesophile); PPA, α-amylase from pig pancreas (homeothermic mesophile); TFA, α-amylase from *Thermobifida fusca* (thermophile); Et-G7-pNP, 4-nitrophenyl-α-D-maltoheptaoside-4,6-O-ethylidene; GdmCl, guanidine hydrochloride; DSC, differential scanning calorimetry; IF, intrinsic fluorescence; CD, circular dichroism.

* Corresponding author. Laboratory of Biochemistry, Institute of Chemistry B6a, B-4000 Liège-Sart Tilman, Belgium. Tel.: +32 4 366 33 43; fax: +32 4 366 33 64.
E-mail address: gfeller@ulg.ac.be (G. Feller).

0300-9084/$ – see front matter © 2012 Elsevier Masson SAS. All rights reserved.
doi:10.1016/j.biochi.2012.05.013

(*Sus scrofa*) pancreas have been extensively studied in the context of protein adaptation to low temperatures [26–30]. It was shown that the high specific activity at low temperatures of cold-adapted enzymes is a key adaptation to compensate for the exponential decrease of chemical reaction rates as temperature is reduced. Such high biocatalytic activity arises from the disappearance of various non-covalent stabilizing interactions, resulting in an improved flexibility of the enzyme conformation and in a weak stability [11,31]. Here, we have extended these earlier observations to the chloride-dependent α-amylases from the ectothermic fruit fly *Drosophila melanogaster* and from the thermophilic actinomycete *Thermobifida fusca*. This series covers nearly all temperatures encountered by living organisms (chloride-dependent α-amylases have not been detected in hyperthermophiles). We report a striking continuum in the functional properties of these enzymes coupled to their structural stability and related to the thermal regime of the source organism.

2. Materials and methods

2.1. Gene cloning

The naturally intronless *amy-p* gene (coding for DMA α-amylase) has been originally amplified by PCR from genomic DNA of *D. melanogaster* using the forward primer 5′-AACTTCCATCTG-GAATCATC-3′ and the reverse primer 5′-TGCTCCCCAGCTGTTTAC-3′ and the resulting PCR fragment was cloned in the pGEM-T Easy vector (pGEM-AmyD). To construct an expression vector, restriction sites *ClaI* and *XbaI* were introduced by PCR in 5′and 3′ of the *amy-p* gene, respectively. The pαH12WT* plasmid, modified with an engineered *Nde*I restriction site at the ATG codon and pGEM-AmyD were digested by *Cla*I and *Xba*I and ligated to produce pα-AmyD in which the residual part of the AHA gene was excised by inverse PCR, producing the pAmyD plasmid. Both pAmyD and pET-22b(+) were digested by *Nde*I/*Hind*III restriction enzymes and ligated to give the pET-AmyD plasmid in which the *amy-p* gene is preceded by the signal peptide of AHA. The nucleotide sequence of this construct is given in the Supplementary Fig. S1.

Based on the sequence of *T. fusca* α-amylase Tfu_0985 (GenBank ID: AAZ55023.1), the TFA gene was re-designed in order to replace the native signal sequence by the signal peptide of AHA and to introduce *Nde*I/*Hind*III restriction sites. The codons were optimized for *E. coli* codon usage and this TFA gene was synthesized by GeneArt (Life Technologies) in a pMA vector. PSTFA_pMA plasmid and pET-22b(+) were digested by *Nde*I/*Hind*III restriction enzymes and fragments were ligated to produce the pET-TFA plasmid. The nucleotide sequence of this construct is given in the Supplementary Fig. S2.

2.2. Enzyme production and purification

The recombinant AHA (pαH12WT* plasmid) was expressed in *Escherichia coli RR1* at 18 °C and purified by DEAE-agarose, Sephadex G-100, and Ultrogel AcA54 column chromatography as previously described [32].

The recombinant DMA α-amylase (pET-AmyD plasmid) was expressed in *E. coli* BL21(DE3) at 18 °C in TB (Terrific Broth) containing 100 mg/l ampicillin and α-amylase production was induced by 0.5 mM IPTG (isopropyl β-D-thiogalactoside) at A_{600} of ~4. After 20 h of induction, cells were recovered by centrifugation at 13,000 g for 50 min at 4 °C. Bacteria were disrupted on an EmulsiFlex-C3 homogenizer (Avestin) in the presence of benzonase and protease inhibitors and cell debris were removed by centrifugation. Purification of DMA was achieved in five steps: (a) An ammonium sulfate precipitation at 85% saturation during 1 h at 4 °C. The precipitate was centrifuged at 23,000 g for 50 min and the pellet was dissolved in a minimum volume of Buffer A (50 mM Tris, 1 mM $CaCl_2$, pH 7,5) and then dialyzed against 2 × 2 L of Buffer B (20 mM Hepes, 20 mM NaCl, pH 7,5). (b) A glycogen precipitation in 40% cold ethanol [33]. After dropwise ethanol addition, the insoluble material was removed by centrifugation and glycogen was added to the supernatant. The pellet was solubilized and dialyzed against Buffer A. (c) The solution was loaded on a Q Sepharose Fast Flow anion exchanger (2.5 × 40 cm) and eluted with a linear NaCl gradient (0–1 M) in Buffer A. (d) Fractions displaying amylolytic activity were concentrated to 10 mL by ultrafiltration using a Millipore polyethersulfone membrane (cutoff 10,000 Da) in an Amicon ultrafiltration unit under 3 bars nitrogen pressure and then loaded on a Sephadex G-100 gel filtration column (2.5 × 100 cm) and eluted with buffer A. (e) The fractions of interest were concentrated to 10 mL by ultrafiltration as described above and then loaded on a Ultrogel AcA54 gel filtration column (2.5 × 100 cm) eluted with buffer A. The recombinant TFA α-amylase (pET-TFA plasmid) was produced and purified as described above except that the Sephadex G-100 step was omitted. PPA was from Roche.

Except where specified, enzyme concentration was determined spectrophotometrically at 280 nm using $A^{0.1\%} = 1.90$ for AHA, 1.71 for DMA, 2.41 for PPA and 1.95 for TFA. Dynamic light scattering was performed on a DynaPro NanoStar instrument (Wyatt Technology Corporation) operated in batch mode at 20 °C and fitted with a laser beam emitting at 658 nm. A globular protein model was used for mass estimation. The N-terminal amino acid sequence of DMA and TFA was determined by automated Edman degradation using a pulsed-liquid-phase protein sequencer Procise 494 (Applied Biosytems) fitted with an online phenylthiohydantoin analyzer. Mass determination was performed by ESI-Q-TOF mass spectrometry (Waters, Micromass) in 25% acetonitrile, 0.5% formic acid.

2.3. Enzyme assays and kinetics

α-Amylase activity was recorded using 3.5 mM 4-nitrophenyl-α-D-maltoheptaoside-4,6-O-ethylidene (Et-G7-pNP) as substrate (Infinity™ Amylase kit, ThermoScientific) and by the dinitrosalicylic acid (DNS) method using 1% soluble starch as substrate [23]. Catalytic concentrations of enzymes were determined by the Bradford assay (Pierce).

The effects of pH on amylolytic activity was determined by the DNS method using a poly-buffer containing 25 mM Na acetate, 25 mM HEPES, 25 mM CHES, 25 mM MES and 20 mM NaCl between pH 3.5 −pH 10.5. Chloride-free α-amylase was prepared by extensive dialysis against 20 mM HEPES-NaOH, pH 7,2. The dissociation constants for Cl^- were obtained from the saturation curves as described [23].

Thermodynamic activation parameters were calculated as described [34] using the equations:

$$\Delta G^{\#} = RT \times (\ln(k_B T/h) - \ln k_{cat}) \quad (1)$$

$$\Delta H^{\#} = E_a - RT \quad (2)$$

$$\Delta S^{\#} = \left(\Delta H^{\#} - \Delta G^{\#}\right)/T \quad (3)$$

where k_B is the Bolzmann constant, h the Planck constant, E_a is the activation energy of the reaction and R the gas constant.

2.4. Differential scanning calorimetry

Measurements were performed using a MicroCal VP-DSC instrument at a scan rate of 60 K h^{-1} and under ~25 psi positive cell pressure. Samples (~2 mg/ml) were dialyzed overnight

against 30 mM MOPS, 50 mM NaCl, 1 mM $CaCl_2$, pH 7.2. For DMA and TFA, both the sample and the reference buffer were brought to 1 M 3-(1-pyridinio)-1-propanesulfonate (*i.e.* a nondetergent sulfobetaine) as detailed [35]. After cell loading, the protein concentration was determined on the remaining sample by the bicinchoninic acid method (Pierce). Thermograms were analyzed according to a non-two-state model in which the melting point T_m, the calorimetric enthalpy ΔH_{cal} and the van't Hoff enthalpy ΔH_{eff} of individual transitions are fitted independently using the MicroCal Origin software (version 7). The magnitude and source of the errors in the T_m and enthalpy values have been discussed elsewhere [36].

2.5. Unfolding recorded by intrinsic fluorescence

Heat-induced unfolding was recorded using an SML-Aminco Model 8100 spectrofluorometer (Spectronic Instruments) at an excitation wavelength of 280 nm and at an emission wavelength of 350 nm (AHA), 340 nm (DMA), 350 nm (PPA) or 336 nm (TFA). A scan rate of 60 K h^{-1} was generated by a Lauda thermostat. GdmCl-induced unfolding was monitored at 20 °C after overnight incubation of the samples at this temperature in 30 mM MOPS, 50 mM NaCl, 1 mM $CaCl_2$, pH 7.2 and increasing GdmCl concentrations on a Perkin–Elmer LS50B spectrofluorometer at protein concentration of ~0.1 mg/ml [30]. The equilibrium condition was ascertained by recording unfolding as a function of time. Least-squares analysis of ΔG° values as a function of GdmCl concentrations allowed estimating the conformational stability in the absence of denaturant, $\Delta G^\circ H_2O$, according to:

$$\Delta G^\circ = \Delta G^\circ_{H_2O} - m\,[\mathrm{GdmCl}] \quad (4)$$

2.6. Circular dichroism

Circular dichroism spectra of the native proteins were recorded using a Jasco J-810 spectropolarimeter under constant nitrogen flow. Spectra in the far UV were recorded at 20 °C in a 0.2 cm cell at a protein concentration of ~50 μg/ml in 5 mM MOPS, 50 mM NaCl, 1 mM $CaCl_2$, pH 7.2. Spectra were averaged over five scans and corrected for the buffer signal. Heat-induced unfolding was recorded under constant nitrogen flow at 222 nm in 30 mM MOPS, 50 mM NaCl, 1 mM $CaCl_2$, pH 7.2 at a scan rate of 60 K h^{-1}. Protein concentration was ~0.1 mg/ml for all proteins. GdmCl-induced unfolding was recorded at 222 nm and 20 °C on the samples used for intrinsic fluorescence.

2.7. GdmCl concentration determination

A Refractometer ATAGO R5000 was used to record the refractive index of each sample in chemical unfolding studies and to calculate the ΔN value (difference in refractive index between the sample and the buffer without GdmCl). This ΔN value allows determination of GdmCl concentration according to [37]:

$$[\mathrm{GdmCl}] = 57.147(\Delta N) + 38.68(\Delta N)^2 - 91,60(\Delta N)^3 \quad (5)$$

2.8. Dynamic quenching of fluorescence

The acrylamide-dependent quenching of intrinsic protein fluorescence was monitored as described [30,38]. The Stern–Volmer quenching constants K_{SV} were calculated according to the relation:

$$F/F_0 = 1 + K_{SV}[Q] \quad (6)$$

where F and F_0 are the fluorescence intensity in the presence and absence of molar concentration of the quencher Q, respectively.

3. Results and discussion

3.1. Production of the recombinant DMA and TFA

The genes coding for DMA and for TFA possess a signal sequence incompatible with periplasmic export in *E. coli*. Accordingly, these sequences have been removed and replaced by the signal peptide of AHA. The production and purification procedures yielded about 50 mg of TFA and 250 mg of DMA per liter of culture. These proteins were found to be homogenous by SDS-PAGE and monodisperse by dynamic light scattering (Supplementary Fig. S3). N-terminal amino acid sequencing of the purified proteins indicated proper cleavage of the signal peptide in DMA whereas the recombinant TFA displayed four additional residues (Ile-Ala-Thr-Ala) from the AHA signal peptide, originating from incorrect processing. Mass determination by ESI-Q-TOF mass spectrometry also revealed the lack of other post-translational modifications and a single homogenous population for both proteins.

3.2. General parameters

Table 1 summarizes some general properties of the investigated enzymes. TFA differs from its homologs by its larger size resulting from an additional C-terminal extension comprising a linker (residues 452–472) and a type 20 carbohydrate-binding module (residues 473–572) [39] rich in tryptophan residues (Supplementary Fig. S4). The optimum pH for starch hydrolysis was found in the range pH 7.2–7.5 for these α-amylases.

3.3. Chloride binding

Both DMA and TFA were predicted to belong to the chloride-dependent α-amylase family on the basis of sequence alignments and conservation of the chloride ligands identified in available crystal structures [20,21]. This was ascertained by removing the chloride ions from the purified proteins by extensive dialysis and performing activation kinetics allowing the determination of the dissociation constants from saturation isotherms. As shown in Table 2, the animal-type DMA and PPA display a high affinity for chloride that can be related to the bidentate coordination by arginine, the main chloride ligand [23]. In this respect, replacement of this ligand by lysine (providing a monodentate coordination) in the bacterial-type AHA and TFA can account for their lower affinity (Supplementary Fig. S5). The weak affinity of AHA has been also

Table 1
General properties of the investigated α-amylases.

Source	Abbreviation	Genbank	CAZy subfamily	residues (n)	Mr (Da)	pI	PDB ID
Pseudoalteromonas haloplanktis	AHA	CAA41481.1	GH13_xx[a]	453	49343.1	4.82	1AQH
Drosophila melanogaster	DMA	CAA28238.1	GH13_15	476	51899.2	5.38	
Sus scrofa	PPA	AAF02828.1	GH13_24	496	55598.3	6.55	1PPI
Thermobifida fusca (native)	TFA	AAZ55023.1	GH13_32	572	61505.0	5.38	
(recombinant)				576	61861.0	5.38	

[a] Currently not classified.

Table 2
Chloride binding by the investigated α-amylases.

α-Amylases	Chloride ligands	Kd (mM)[a]
AHA	$172Arg^{NH2}$ $262Asn^{ND2}$ $300Lys^{NZ}$	6.70 ± 0.22[b]
DMA	$184Arg^{NH2}$ $286Asn^{ND2}$ $325Arg^{NH1\text{-}NH2}$	0.22 ± 0.01
PPA	$195Arg^{NH2}$ $298Asn^{ND2}$ $337Arg^{NH1\text{-}NH2}$	0.29 ± 0.01[c]
TFA	$184Arg^{NH2}$ $278Asn^{ND2}$ $312Lys^{NZ}$	1.22 ± 0.02

[a] Data at 25 °C except for TFA (40 °C).
[b] Data similar to [40].
[c] Data from [57].

related to the flexible conformation of this psychrophilic enzyme [29,40] and it appears that the higher affinity of TFA (versus AHA) could be the result of a more stable and compact conformation of this thermophilic enzyme.

3.4. Temperature dependence of activity and conformation

Fig. 1a depicts the thermodependence of activity, using starch as substrate, of the four investigated enzymes. The psychrophilic AHA retains a high relative activity at low temperature in order to maintain catalysis in the cold, whereas the thermophilic TFA is almost inactive at low temperatures, as generally observed [41]. There is a clear shift of the temperature range for efficient catalysis (left limb of the curves) and of the temperature for maximal activity (Table 3) with the environmental/physiological temperatures of the source organisms. When the turnover numbers are compared at the relevant temperature for the source organisms (Table 3), the k_{cat} values exponentially increase from the psychrophilic to both mesophilic and the thermophilic enzymes (Supplementary Fig. S6). This result somewhat contradicts the "corresponding states" hypothesis [42] suggesting that enzymes have evolved their functionality to reach similar activity at their respective environmental temperatures. In the case of the psychrophilic AHA, cold-adaptations do not fully compensate activity when compared with both mesophilic α-amylases. As a matter of fact, microorganisms thriving at near-freezing temperatures grow much more slowly than their mesophilic counterpart at 37 °C. On the other hand, the thermophilic enzyme benefits of the high temperature of its environment to boost its activity towards high k_{cat} values. This can partly explain the powerful degrading capacity of *T. fusca* in hot environments [39]. The exponential increase of activity at relevant temperatures suggests that the thermal energy of the environment plays a crucial role in enzyme activity that is not averaged or normalized by adaptive mechanisms. However, similar comparisons in other homologous series are required before to conclude.

Fig. 1b and c display the heat-induced unfolding of the tertiary structures (as recorded by intrinsic fluorescence, IF) and of the secondary structures (as recorded by circular dichroism, CD). In all cases, these α-amylases unfold cooperatively, i.e. with simultaneous melting of both tertiary and secondary structures. The melting point T_m of the structural conformation (Table 3) also increases with increasing environmental/physiological temperatures of the source organisms. Fig. 1 also indicates that the activity of both mesophilic enzymes and of the thermophilic α-amylase is heat-inactivated when their structure starts to melt, as judged by the correspondence between the maximal temperature for activity and the unfolding curves. This is in sharp contrast with the psychrophilic

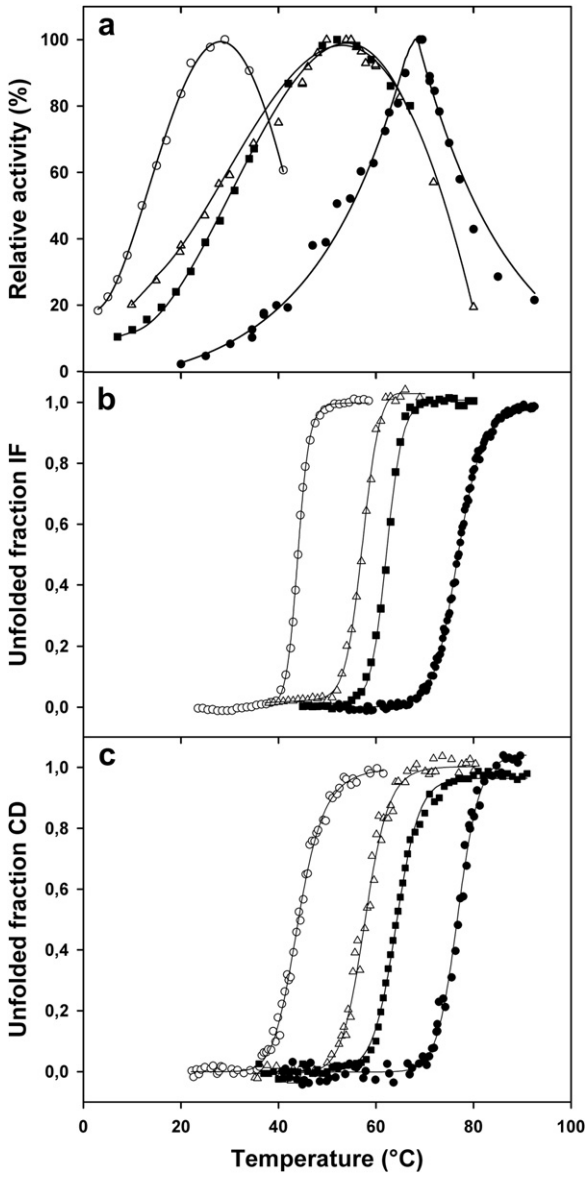

Fig. 1. Temperature dependence of activity (a) and heat-induced unfolding recorded by fluorescence (b) and circular dichroism (c). From left to right: the psychrophilic AHA (open circles), the ectothermic DMA (open triangles), the homeothermic PPA (closed squares) and the thermophilic TFA (closed circles). In panels (a) and (b), data for AHA and PPA are from [32,38].

Table 3
Activity and stability of the investigated α-amylases.

α-Amylases	Temperature of maximal activity	k_{cat} at physiological temperature		Melting temperature T_m	
	(°C)	(s^{-1})	(°C)	Tertiary structure	Secondary structures
				(°C)	(°C)
AHA	29	179 ± 9	5	44.1	44.1
DMA	54	280 ± 13	20	57.7	57.7
PPA	54	518 ± 22	37	65.0	65.0
TFA	72	1457 ± 37	55	76.8	76.9

AHA which is heat-inactivated before any detectable structural change. It has been previously argued that a very flexible (and therefore heat-labile) active site is required for activity at low temperatures [11,31].

3.5. Thermodynamic parameters of activation

The thermodynamic parameters of activation have been calculated from Arrhenius plots of the exponential rise of activity with temperature, providing the activation energy E_a, and are reported in Table 4. When the four enzymes are compared at an identical temperature, the k_{cat} values clearly reflect the adaptive nature of activity that decreases from the psychrophilic to the thermophilic α-amylases, as also inferred from Fig. 1a. This is translated into increasing values of the Gibbs free energy of activation $\Delta G^{\#}$, which is an inverse function of k_{cat} in the transition state formalism (Eq. (1)). Amongst the activation parameters, the variation of activation enthalpy $\Delta H^{\#}$ appears to be the most instructive. Indeed, this parameter reflects two aspects. Firstly, it depicts the temperature dependence of the enzymatic reaction [43]: for a given variation of temperature, the activity of the psychrophilic enzyme is less modified than that of the thermophilic one. This ensures that a decrease in temperature will moderately reduce the activity of the psychrophilic enzyme therefore maintaining a high activity at low temperature, whereas an increase in temperature will sharply activate the thermophilic enzyme for maximal activity at high temperature. It should be noted that the ectothermic and homeothermic α-amylases display intermediate values in close relation with their physiological temperatures. Secondly, the $\Delta H^{\#}$ parameter is related to the number of enthalpically-driven weak interactions that have to be broken to reach the activated state [34]. It follows that the number of such interactions that are disrupted increases in the enzyme series, from a low number in the psychrophilic enzyme to a high number in the thermophilic α-amylase. It should be stresses that, in this respect, there is a striking correlation between the $\Delta H^{\#}$ parameter and the stability of the four enzymes which arises from increased numbers of stabilizing interactions. The entropic contribution $T\Delta S^{\#}$ to the free energy of activation is also worth commenting. In the case of the psychrophilic enzyme, the large and negative variation of activation entropy has been related to a transition from a flexible and mobile active site in the ground state, to a more ordered active site in the activated complex. This hypothesis was supported by experimental evidences using a transition state analog [30,38]. In Table 4, the progressive evolution of entropy in parallel with stability can be tentatively related to a progressively more stable free enzyme in the ground state. If calculated at the relevant environmental/physiological temperatures given in Table 3, all these activation parameters remain qualitatively similar (Supplementary Table S1).

3.6. Substrate binding

The kinetic parameters for hydrolysis of the chromogenic substrate Et-G7-pNP are reported in Table 5. It has been previously argued that a high activity at low or moderate temperature is gained at the expense of affinity for the substrate [29,41]. This allows a reduction of the activation free energy barrier (and therefore increased k_{cat} values) by lowering the magnitude of the energy pit of the enzyme–substrate complex. This is supported in Table 5 by the simultaneous decrease of k_{cat} and K_m values, from AHA to DMA and PPA. Furthermore, the decrease of K_m values suggests that the active site dynamics also decrease from AHA to DMA and PPA. By contrast, the affinity of TFA is weak and the low k_{cat}/K_m ratio indicates that Et-G7-pNP is a poor substrate for the thermophilic enzyme. It should be mentioned that amongst the 24 residues forming the catalytic cleft [44] (strictly conserved in AHA, DMA and PPA), 6 are substituted in TFA (Supplementary Fig. S4). These substitutions possibly account for the alteration in substrate binding by TFA. It should also be mentioned that TFA appears to be a maltotriose-forming α-amylase [45], therefore differing in product release.

Table 4
Thermodynamic parameters of activation at 15 °C (Standard errors are ± 1% on $\Delta G^{\#}$ and <10% on both $\Delta H^{\#}$ and $\Delta S^{\#}$).

	k_{cat} (s^{-1})	E_a (kcal mol^{-1})	$\Delta G^{\#}$ (kcal mol^{-1})	$\Delta H^{\#}$ (kcal mol^{-1})	$T\Delta S^{\#}$ (kcal mol^{-1})
AHA[a]	392 ± 18	8.9	13.4	8.3	−5.1
DMA	150 ± 6	10.9	14.0	10.3	−3.6
PPA[a]	141 ± 4	12.0	14.0	11.5	−2.5
TFA	42 ± 2	22.9	14.7	22.4	7.7

[a] Data from [28].

Table 5
Kinetic parameters at 25 °C for Et-G7-pNP hydrolysis.

	k_{cat} (s^{-1})	K_m (μM)	k_{cat}/K_m (s^{-1} μM^{-1})
AHA[a]	675 ± 31	223 ± 15	3.0
DMA	364 ± 15	130 ± 8	2.8
PPA[b]	291 ± 8	65 ± 4	4.5
TFA	153 ± 4	260 ± 10	0.6

[a] Data similar to [28].
[b] Data from [28].

3.7. Equilibrium unfolding in GdmCl

The resistance towards chemical denaturation using GdmCl (guanidinium hydrochloride) was probed by equilibrium unfolding recorded by fluorescence and circular dichroism (Fig. 2, Table 6). Both methods indicate a single cooperative transition as well as a cooperative unfolding of secondary and tertiary structures in all enzymes. The GdmCl concentration for half denaturation ($C_{1/2}$ value in Table 6) increases from AHA to TFA, while the large m value of AHA reflects its sharp cooperative unfolding. Estimation of the conformational stability in the absence of denaturant ($\Delta G^{\circ}_{H_2O}$) in Table 6 shows that stability increases with the thermal regime of the source organism. However, the stability determined by GdmCl unfolding for PPA and TFA is very close (Fig. 2), in contrast with their thermal stability (Fig. 1). This indicates unusual differences between thermal denaturation and chemical unfolding in both proteins.

3.8. Differential scanning microcalorimetry

In order to gain deeper insights into stability of these α-amylases, thermal unfolding was recorded by differential scanning calorimetry (DSC). Both mesophilic and the thermophilic proteins required the addition of a nondetergent sulfobetaine to avoid heat-induced aggregation. The normalized thermograms are displayed in Fig. 3 and the related thermodynamic parameters are given in Table 7. The melting temperature T_m (top of the main transition) increases from the psychrophilic AHA to the thermophilic TFA (Fig. 3) and closely corresponds to the values recorded by spectroscopic methods (Fig. 1, Table 3). Furthermore, the calorimetric enthalpy (ΔH_{cal}, heat absorbed during unfolding calculated from the area under the transition) also increases from AHA to TFA (Table 7). This ΔH_{cal} value corresponds to the sum of all enthalpically-driven interactions that have to be broken for unfolding and precisely quantify the enthalpic stability of these α-

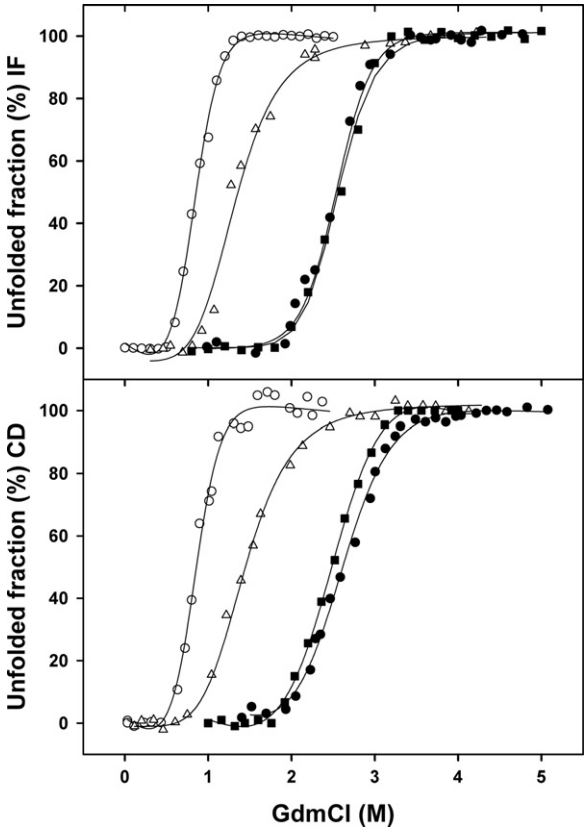

Fig. 2. Equilibrium unfolding in GdmCl recorded by intrinsic fluorescence (IF, upper panel) and circular dichroism (CD, lower panel). From left to right: the psychrophilic AHA (open circles), the ectothermic DMA (open triangles), the homeothermic PPA (closed squares) and the thermophilic TFA (closed circles). In the upper panel, data for PPA are from [38].

amylases. Fig. 3 also shows that unfolding of mesophilic and the thermophilic proteins is asymmetric and can be deconvoluted into two cooperative transitions that are not detected by spectroscopic methods. Accordingly, the cold-adapted AHA is uniformly unstable (single cooperative transition) whereas the mesophilic and thermophilic proteins are characterized by the appearance of thermodynamic domains with increased stability, in parallel to the protein thermal origin.

The thermophilic TFA differs by the occurrence of a small, very stable transition at 85 °C. Two explanations can be proposed for this unusual transition. *i*) This domain can correspond to the unfolding of the additional C-terminal carbohydrate-binding module in TFA, although spectroscopic methods fail to detect such transition. *ii*) It has been shown that some thermophilic proteins retain residual structure in the unfolded state [46]. This residual structure reduces the entropy of the unfolded state and therefore increases the stability of the native state. The additional DSC transition in TFA can be regarded as the melting of such residual structure at high temperature.

Table 6
Equilibrium unfolding parameters in GdmCl at 20 °C recorded by intrinsic fluorescence (IF) and circular dichroism (CD).

Protein	AHA		DMA		PPA		TFA	
	IF	CD	IF	CD	IF[a]	CD	IF	CD
$C_{1/2}$ (M)	0.82	0.83	1.34	1.45	2.5	2.48	2.54	2.59
m (kcal mol^{-1} M^{-1})	4.32	4.37	2.43	2.73	2.7	2.75	2.96	2.75
$\Delta G°_{H_2O}$ (kcal mol^{-1})	3.66	3.87	3.80	3.94	6.9	6.82	7.39	7.14

[a] Data from [38].

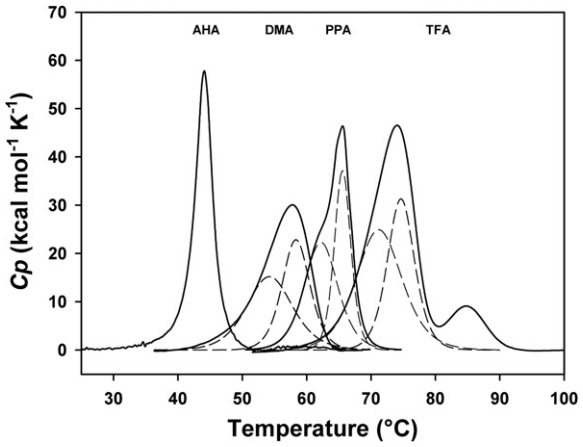

Fig. 3. Thermal unfolding of α-amylases recorded by differential scanning calorimetry. The individual thermograms are identified at the top of the transitions. Dashed lines are deconvolutions of the main transition into two cooperative units in mesophilic and thermophilic proteins. In TFA, note the additional transition melting around 85 °C. Data for PPA are from [28].

3.9. Stability curves

On the basis of the microcalorimetric parameters (Table 7), the stability curves have been calculated according to the relation [47]:

$$\Delta G(T) = \Delta H_{cal}(1 - T/T_m) + \Delta Cp(T - T_m) - T\Delta Cp \ln(T/T_m) \quad (7)$$

In the present case, a ΔCp value of 8.47 kcal mol^{-1} K^{-1} measured for various α-amylases [32] was used and the extra stability domain of TFA was excluded from calculations. These stability curves (Fig. 4) correspond to the work required to disrupt the native state at any temperature. The stability curve of AHA has been validated experimentally [32] whereas the curves for the other α-amylases are estimations due to the non-two-state unfolding of their structures (dashed in Fig. 3). By definition, the ΔG value is nil at the melting point T_m. It can be seen in Fig. 4 that the increasing stability of the α-amylases is reached by uplifting the curves towards higher free energy values from AHA to TFA. The thermodynamic implications of these curves have been discussed elsewhere [41] and fit the present observations. For instance, the maximal stability of all α-amylases is reached near room temperature, possibly because the hydrophobic effect is optimal in this range [48]. From an evolutionary perspective, the adaptive variations in stability appear to be restrained by enthalpic stabilization (ΔH_{cal}, T_m) as no significant alteration of the curve shape (minor displacement of maximal stability, no slope modification), except uplifting, are detected in Fig. 4.

3.10. Dynamic fluorescence quenching

The conformational flexibility of the α-amylases was probed by dynamic fluorescence quenching of aromatic residues [30,38].

Table 7
Thermodynamic parameters of stability recorded by microcalorimetry (Standard errors are ± 0.05 °C on T_m and ±2% on ΔH_{cal}).

		T_m (°C)	ΔH_{cal} (kcal mol^{-1})
AHA		44.0	214
DMA		57.7	274
PPA[a]		65.6	295
TFA	(1)[b]	74.0	415
	(2)	84.7	46

[a] Data from [28].
[b] Main (1) and minor (2) transitions in Fig. 3.

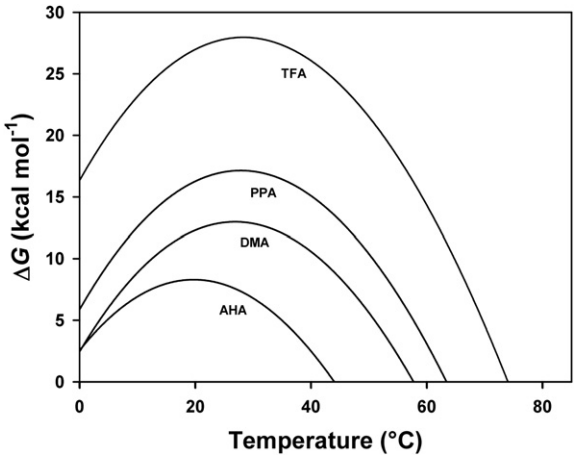

Fig. 4. Stability curves calculated from DSC data. The Gibbs free energy of unfolding corresponds to the work required to unfold the native state as a function of temperature. The increased stability of the α-amylases and of T_m (at $\Delta G = 0$) is essentially gained via uplifting the curves towards higher free energy values. Data for AHA and PPA are from [38].

Increased concentrations of a small quencher molecule (acrylamide) were used to probe the accessibility of tryptophan residues within the proteins. The decrease of fluorescence arising from diffusive collisions between acrylamide and tryptophans reflects the ability of acrylamide to penetrate the structure and provides an index of protein permeability. The difference between the slopes of Stern–Volmer plots at 30 °C and 4 °C illustrates the variations in protein structural permeability with an increase in temperature (Fig. 5). In the case of AHA, DMA and PPA, the recorded decrease in permeability correlates with the increase in stability. This reveals that when stability increases in this series, the proteins are characterized by progressively more compact conformation undergoing reduced micro-unfolding events of the native state and shorter native state fluctuations. However, TFA does not integrate the relation in the series (slope between DMA and PPA in Fig. 5). This could be related to its additional C-terminal domain rich in tryptophan residues (Supplementary Fig. S4) that can interfere in this fluorescence-based experiment by the presence of solvent- exposed tryptophans (as expected in a carbohydrate-binding module). Nevertheless, the thermostable α-amylase from *B. amyloliquefaciens* displayed very limited quenching under similar conditions [38], suggesting that the flexibility–stability relationship can be extended to heat-stable proteins on the basis of fluorescence quenching.

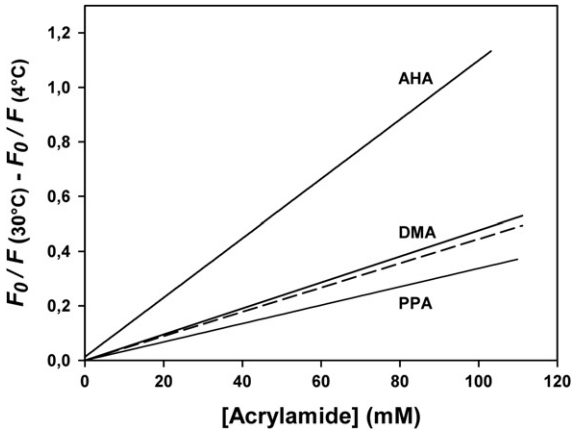

Fig. 5. Variation of fluorescence quenching by acrylamide between 4 and 30 °C. Data for TFA are dashed and data for PPA are from [38]. The slope of the plots is proportional to the permeability of the proteins towards acrylamide.

4. Conclusions

We report here a close correlation between thermal stability and the environmental/physiological temperature in mesophilic and extremophilic α-amylases. While the requirement for a high stability is obvious for the thermophilic protein, this correlation for all α-amylases cannot be fortuitous in regard of previous examples [11,16,41,42]. It has been proposed that this correlation is the result of a genetic drift related to the lack of selective pressure for stable proteins at individual environmental temperatures [49]. More importantly, it has been also argued that protein dynamics has to be preserved at environmental temperatures in order to maintain a functional state. Furthermore, such dynamic properties are inversely linked with structural stability: the lower the mobility of the protein structure, the higher its stability [50–53], as also indicated here by fluorescence quenching. Such balance between stability, dynamics and activity clearly accounts for the continuum of the properties observed in the investigated α-amylases. The thermodependence of activity, the kinetic parameters and the activations parameters support these activity-stability trade-offs. In the case of the psychrophilic AHA, there is notably a strong selective pressure for a high activity at low and moderate temperatures. This selection should be less essential for mesophilic and the thermophilic α-amylases that benefit from thermally-induced activity: this can tentatively explain the exponential rise of k_{cat} values at relevant temperature noted in the four α-amylases.

The enzyme functional properties are intimately governed by protein motions and conformational changes. In this respect, increasing attention is currently given to the pathways of adaptive protein evolution [54], the evolution of protein conformational changes [55] and to the mutational adjustments of conformational energy landscapes [56]. For instance, we have recently shown that mesophilic stability, activity and dynamics can be engineered in the psychrophilic AHA by introducing key adaptive substitutions [30]. The availability of the crystal structure of DMA and TFA will certainly further improve our understanding of temperature-driven adaptations of the enzyme function.

Acknowledgments

This work was supported by grants from the FRS-FNRS, Belgium (Fonds de la Recherche Fondamentale et Collective, contract number 2.4535.08) to G.F., the Belgian program of Interuniversity Attraction Poles initiated by the Federal Office for Scientific, Technical and Cultural Affaires (PAI n° P6/19) and from the Centre National de la Recherche Scientifique (France) to J.-L.D.L. AC was a FRIA fellow during this work.

Appendix A. Supplementary material

Supplementary data associated with this article can be found, in the online version, at doi:10.1016/j.biochi.2012.05.013.

References

[1] J.W. Deming, Psychrophiles and polar regions, Curr. Opin. Microbiol. 5 (2002) 301–309.
[2] K. Takai, K. Nakamura, T. Toki, U. Tsunogai, M. Miyazaki, J. Miyazaki, H. Hirayama, S. Nakagawa, T. Nunoura, K. Horikoshi, Cell proliferation at 122 degrees C and isotopically heavy CH4 production by a hyperthermophilic methanogen under high-pressure cultivation, Proc. Natl. Acad. Sci. U.S.A. 105 (2008) 10949–10954.
[3] C. Gerday, N. Glansdorff, Physiology and Biochemistry of Extremophiles, ASM Press, Washington, D.C, 2007.

[4] K. Horikoshi, G. Antranikian, A.T. Bull, F.T. Robb, K.O. Stetter (Eds.), Extremophiles Handbook, Springer Verlag, Tokyo, Berlin, Heidelberg, 2011.
[5] B. Boussau, S. Blanquart, A. Necsulea, N. Lartillot, M. Gouy, Parallel adaptations to high temperatures in the Archaean eon, Nature 456 (2008) 942–945.
[6] K.A. Maher, D.J. Stevenson, Impact frustration of the origin of life, Nature 331 (1988) 612–614.
[7] M. Di Giulio, The universal ancestor and the ancestor of bacteria were hyperthermophiles, J. Mol. Evol. 57 (2003) 721–730.
[8] M. Levy, S.L. Miller, The stability of the RNA bases: implications for the origin of life, Proc. Natl. Acad. Sci. U.S.A. 95 (1998) 7933–7938.
[9] J. Attwater, A. Wochner, V.B. Pinheiro, A. Coulson, P. Holliger, Ice as a protocellular medium for RNA replication, Nat. Commun. 1 (2010) 76. doi:10.1038/ncomms1076.
[10] C. Vieille, G.J. Zeikus, Hyperthermophilic enzymes: sources, uses, and molecular mechanisms for thermostability, Microbiol. Mol. Biol. Rev. 65 (2001) 1–43.
[11] G. Feller, C. Gerday, Psychrophilic enzymes: hot topics in cold adaptation, Nat. Rev. Microbiol. 1 (2003) 200–208.
[12] G.S. Bell, R.J. Russell, H. Connaris, D.W. Hough, M.J. Danson, G.L. Taylor, Stepwise adaptations of citrate synthase to survival at life's extremes. From psychrophile to hyperthermophile, Eur. J. Biochem. 269 (2002) 6250–6260.
[13] D. Georlette, B. Damien, V. Blaise, E. Depiereux, V.N. Uversky, C. Gerday, G. Feller, Structural and functional adaptations to extreme temperatures in psychrophilic, mesophilic, and thermophilic DNA ligases, J. Biol. Chem. 278 (2003) 37015–37023.
[14] E. Bae, G.N. Phillips Jr., Structures and analysis of highly homologous psychrophilic, mesophilic, and thermophilic adenylate kinases, J. Biol. Chem. 279 (2004) 28202–28208.
[15] A. Linden, M. Wilmanns, Adaptation of class-13 alpha-amylases to diverse living conditions, ChemBioChem 5 (2004) 231–239.
[16] N. Coquelle, E. Fioravanti, M. Weik, F. Vellieux, D. Madern, Activity, stability and structural studies of lactate dehydrogenases adapted to extreme thermal environments, J. Mol. Biol. 374 (2007) 547–562.
[17] B.L. Cantarel, P.M. Coutinho, C. Rancurel, T. Bernard, V. Lombard, B. Henrissat, The carbohydrate-active EnZymes database (CAZy): an expert resource for Glycogenomics, Nucleic Acids Res. 37 (2009) D233–D238.
[18] S. Janecek, Alpha-Amylase family: molecular biology and evolution, Prog. Biophys. Mol. Biol. 67 (1997) 67–97.
[19] S. Janecek, Sequence similarities and evolutionary relationships of microbial, plant and animal alpha-amylases, Eur. J. Biochem. 224 (1994) 519–524.
[20] S. D'Amico, C. Gerday, G. Feller, Structural similarities and evolutionary relationships in chloride-dependent alpha-amylases, Gene 253 (2000) 95–105.
[21] J.L. Da Lage, G. Feller, S. Janecek, Horizontal gene transfer from Eukarya to bacteria and domain shuffling: the alpha-amylase model, Cell. Mol. Life Sci. 61 (2004) 97–109.
[22] J.L. Da Lage, E.G. Danchin, D. Casane, Where do animal alpha-amylases come from? An interkingdom trip, FEBS Lett. 581 (2007) 3927–3935.
[23] G. Feller, O. Bussy, C. Houssier, C. Gerday, Structural and functional aspects of chloride binding to *Alteromonas haloplanctis* alpha-amylase, J. Biol. Chem. 271 (1996) 23836–23841.
[24] M. Qian, H. Ajandouz el, F. Payan, V. Nahoum, Molecular basis of the effects of chloride ion on the acid-base catalyst in the mechanism of pancreatic alpha-amylase, Biochemistry 44 (2005) 3194–3201.
[25] R. Maurus, A. Begum, L.K. Williams, J.R. Fredriksen, R. Zhang, S.G. Withers, G.D. Brayer, Alternative catalytic anions differentially modulate human alpha-amylase activity and specificity, Biochemistry 47 (2008) 3332–3344.
[26] N. Aghajari, G. Feller, C. Gerday, R. Haser, Structures of the psychrophilic *Alteromonas haloplanctis* α-amylase give insights into cold adaptation at a molecular level, Structure 6 (1998) 1503–1516.
[27] S. D'Amico, C. Gerday, G. Feller, Structural determinants of cold adaptation and stability in a large protein, J. Biol. Chem. 276 (2001) 25791–25796.
[28] S. D'Amico, C. Gerday, G. Feller, Temperature adaptation of proteins: engineering mesophilic-like activity and stability in a cold-adapted alpha-amylase, J. Mol. Biol. 332 (2003) 981–988.
[29] S. D'Amico, J.S. Sohier, G. Feller, Kinetics and energetics of ligand binding determined by microcalorimetry: insights into active site mobility in a psychrophilic alpha-amylase, J. Mol. Biol. 358 (2006) 1296–1304.
[30] A. Cipolla, S. D'Amico, R. Barumandzadeh, A. Matagne, G. Feller, Stepwise adaptations to low temperature as revealed by multiple mutants of psychrophilic alpha-amylase from Antarctic Bacterium, J. Biol. Chem. 286 (2011) 38348–38355.
[31] K.S. Siddiqui, R. Cavicchioli, Cold-adapted enzymes, Annu. Rev. Biochem. 75 (2006) 403–433.
[32] G. Feller, D. d'Amico, C. Gerday, Thermodynamic stability of a cold-active α-amylase from the Antarctic bacterium *Alteromonas haloplanctis*, Biochemistry 38 (1999) 4613–4619.
[33] M. Schramm, A. Loyter, Purification of alpha-amylases by precipitation of amylase-glycogen complexes, Methods Enzymol. 8 (1966) 533–537.
[34] T. Lonhienne, C. Gerday, G. Feller, Psychrophilic enzymes: revisiting the thermodynamic parameters of activation may explain local flexibility, Biochim. Biophys. Acta 1543 (2000) 1–10.
[35] S. D'Amico, G. Feller, A nondetergent sulfobetaine improves protein unfolding reversibility in microcalorimetric studies, Anal. Biochem. 385 (2009) 389–391.
[36] A. Matouschek, J.M. Matthews, C.M. Johnson, A.R. Fersht, Extrapolation to water of kinetic and equilibrium data for the unfolding of barnase in urea solutions, Protein Eng. 7 (1994) 1089–1095.
[37] C.N. Pace, Determination and analysis of urea and guanidine hydrochloride denaturation curves, Methods Enzymol. 131 (1986) 266–280.
[38] S. D'Amico, J.C. Marx, C. Gerday, G. Feller, Activity-stability relationships in extremophilic enzymes, J. Biol. Chem. 278 (2003) 7891–7896.
[39] A. Lykidis, K. Mavromatis, N. Ivanova, I. Anderson, M. Land, G. DiBartolo, M. Martinez, A. Lapidus, S. Lucas, A. Copeland, P. Richardson, D.B. Wilson, N. Kyrpides, Genome sequence and analysis of the soil cellulolytic actinomycete *Thermobifida fusca* YX, J. Bacteriol. 189 (2007) 2477–2486.
[40] G. Feller, F. Payan, F. Theys, M. Qian, R. Haser, C. Gerday, Stability and structural analysis of α-amylase from the Antarctic psychrophile *Alteromonas haloplanctis* A23, Eur. J. Biochem. 222 (1994) 441–447.
[41] G. Feller, Protein stability and enzyme activity at extreme biological temperatures, J. Phys.-Condens. Mat. 22 (2010). doi:10.1088/0953–8984/1022/1032/323101.
[42] G.N. Somero, Proteins and temperature, Annu. Rev. Physiol. 57 (1995) 43–68.
[43] P.A. Fields, G.N. Somero, Hot spots in cold adaptation: localized increases in conformational flexibility in lactate dehydrogenase A(4) orthologs of Antarctic notothenioid fishes, Proc. Natl. Acad. Sci. U.S.A. 95 (1998) 11476–11481.
[44] N. Aghajari, M. Roth, R. Haser, Crystallographic evidence of a transglycosylation reaction: ternary complexes of a psychrophilic alpha-amylase, Biochemistry 41 (2002) 4273–4280.
[45] C.H. Yang, W.H. Liu, Cloning and characterization of a maltotriose-producing alpha-amylase gene from *Thermobifida fusca*, J. Ind. Microbiol. Biotechnol. 34 (2007) 325–330.
[46] S. Robic, M. Guzman-Casado, J.M. Sanchez-Ruiz, S. Marqusee, Role of residual structure in the unfolded state of a thermophilic protein, Proc. Natl. Acad.Sci. U.S.A. 100 (2003) 11345–11349.
[47] P.L. Privalov, Stability of proteins: small globular proteins, Adv. Protein Chem. 33 (1979) 167–241.
[48] S. Kumar, C.J. Tsai, R. Nussinov, Maximal stabilities of reversible two-state proteins, Biochemistry 41 (2002) 5359–5374.
[49] P.L. Wintrode, F.H. Arnold, Temperature adaptation of enzymes: lessons from laboratory evolution, Adv. Protein Chem. 55 (2000) 161–225.
[50] P.L. Privalov, Stability of proteins. Proteins which do not present a single cooperative system, Adv. Protein Chem. 35 (1982) 1–104.
[51] P. Zavodszky, J. Kardos, A. Svingor, G.A. Petsko, Adjustment of conformational flexibility is a key event in the thermal adaptation of proteins, Proc. Natl. Acad. Sci. U.S.A. 95 (1998) 7406–7411.
[52] M. Tehei, B. Franzetti, D. Madern, M. Ginzburg, B.Z. Ginzburg, M.T. Giudici-Orticoni, M. Bruschi, G. Zaccai, Adaptation to extreme environments: macromolecular dynamics in bacteria compared in vivo by neutron scattering, EMBO Rep. 5 (2004) 66–70.
[53] M. Tehei, D. Madern, B. Franzetti, G. Zaccai, Neutron scattering reveals the dynamic basis of protein adaptation to extreme temperature, J. Biol. Chem. 280 (2005) 40974–40979.
[54] J.D. Bloom, F.H. Arnold, In the light of directed evolution: pathways of adaptive protein evolution, Proc. Natl. Acad. Sci. U. S. A 106 (2009) 9995–10000.
[55] J. Jeon, H.J. Nam, Y.S. Choi, J.S. Yang, J. Hwang, S. Kim, Molecular evolution of protein conformational changes revealed by a network of evolutionarily coupled residues, Mol. Biol. Evol. 28 (2011) 2675–2685.
[56] J.P. Colletier, A. Aleksandrov, N. Coquelle, S. Mraihi, E. Mendoza-Barbera, M. Field, D. Madern, Sampling the conformational energy landscape of a hyperthermophilic protein by engineering key substitutions, Mol. Biol. Evol. (2012). doi:10.1093/molbev/mss015.
[57] A. Levitzki, M.L. Steer, The allosteric activation of mammalian alpha-amylase by chloride, Eur. J. Biochem. 41 (1974) 171–180.

Supplementary Material to

Temperature adaptations in psychrophilic, mesophilic and thermophilic chloride-dependent alpha-amylases

Alexandre Cipolla [a], François Delbrassine [a], Jean-Luc Da Lage [b] and Georges Feller [a]*

[a] *Laboratory of Biochemistry, Center for Protein Engineering, University of Liège, B-4000 Liège-Sart Tilman, Belgium*

[b] *UPR9034 Evolution, Génomes et Spéciation, CNRS, F-91198 Gif-sur-Yvette, France and Université Paris-Sud, 91405 Orsay cedex, France*

*Corresponding author
G. Feller, Laboratory of Biochemistry, Institute of Chemistry B6a, B-4000 Liège-Sart Tilman, Belgium, Tel. +32 4 366 33 43; Fax. +32 4 366 33 64; E-Mail: gfeller@ulg.ac.be

Abbreviations: AHA: α-amylase from *Pseudoalteromonas haloplanktis* (psychrophile); DMA: α-amylase from *Drosophila melanogaster* (ectothermic mesophile); PPA: α-amylase from pig pancreas (homeothermic mesophile); TFA: α-amylase from *Thermobifida fusca* (thermophile)

Nde I

CATATGAAACTCAATAAAATAATCACCACCGCAGGTTTAAGCCTAGGGTTGCTCTTACCTAGCATTGCGACTGCTCAATT
CGACACCAACTACGCATCCGGTCGTAGTGGAATGGTCCACCTCTTCGAGTGGAAGTGGGACGACATCGCTGCCGAGTGCG
AGAACTTCCTGGGACCCAATGGCTACGCCGGTGTTCAGGTCTCCCCTGTGAACGAGAACGCCGTCAAGGACAGCCGCCCC
TGGTGGGAACGTTACCAGCCCATCTCCTACAAGCTGGAGACCCGCTCCGGAAACGAAGAGCAGTTCGCCAGCATGGTCAA
GCGCTGCAACGCCGTCGGAGTGCGCACCTACGTGGACGTGGTCTTCAACCACATGGCCGCCGACGGAGGCACCTACGGCA
CTGGCGGCAGCACCGCCAGCCCCAGCAGCAAGACCTATCCCGGAGTGCCCTACTCCTCGCTGGACTTCAACCCGACCTGC
GCCATCAGCAACTACAACGACGCCAACGAGGTGCGCAACTGCGAGCTGGTCGGTCTGCGCGACCTTAACCAGGGCAACTC
CTACGTGCAGGACAAGGTGGTCGAGTTCCTGGACCATCTGATTGATCTCGGCGTGGCCGGATTCCGCGTGGACGCCGCCA
AGCACATGTGGCCCGCCGACCTGGCCGTCATCTATGGCCGCCTCAAGAACCTGAACACCGACCACGGCTTCGCCTCGGGA
TCCAAGGCGTACATCGTCCAGGAGGTCATCGACATGGGCGGCGAGGCCATCAGCAAGTCCGAGTACACCGGACTGGGCGC
CATCACCGAGTTCCGCCACTCCGACTCCATCGGCAAGGTCTTCCGCGGCAAGGACCAGCTGCAGTATCTGACCAACTGGG
GCACCGCCTGGGGCTTCGCTGCCTCCGACCGCTCCCTGGTATTCGTCGACAACCACGACAACCAGCGCGGACATGGAGCA
GGAGGCGCCGACGTGCTGACCTACAAGGTGCCCAAGCAGTACAAGATGGCCTCCGCCTTTATGCTGGCGCACCCATTCGG
CACTCCCCGCGTGATGTCCTCCTTCTCCTTCACGGACACCGATCAGGGCCCGCCCACCACCGACGGCCACAACATCGCCT
CGCCCATCTTCAATAGCGACAACTCCTGCAGCGGCGGCTGGGTGTGCGAGCACCGCTGGCGCCAGATCTACAACATGGTG
GCCTTCCGAAACGCCGTGGGCTCGGACGAGATCCAGAACTGGTGGGACAACGGCAGCAACCAGATCTCCTTCAGCCGAGG
CAGCCGCGGCTTCGTGGCCTTCAACAACGACAACTACGACCTGAACAGCTCCCTGCAGACGGGCCTGCCCGCCGGCACCT
ACTGCGACGTCATCTCCGGCTCCAAGAGCGGTTCCTCCTGCACGGGCAAGACCGTCACCGTCGGATCCGACGGACGGGCT
TCCATCAACATTGGCAGCTCCGAGGACGACGGAGTGCTGGCCATTCACGTCAACGCCAAGTTGTAATCTAGAGTCGACCT
GCAGCCCAAGCTT

Stop *Hind* III

Supplementary Figure S1: Nucleotide sequence of DMA engineered for *E. coli* expression

---

Nde I

CATATGAAACTCAATAAAATAATCACCACCGCAGGTTTAAGCCTAGGGTTGCTCTTACCTAGCATTGCGA
CTGCTGCTCCGTCTGGAAATCGTGACGTCATCGTCCACCTGTTCCAATGGCGCTGGAAAAGCATTGCTGA
CGAATGTCGTACCACTCTGGGTCCACATGGGTTTGGCGCTGTCCAAGTGTCTCCTCCTCAAGAGCACGTT
GTACTGCCTGCTGAAGATTATCCTTGGTGGCAGGACTATCAGCCGGTTTCCTATAAACTGGATCAGACTC
GTCGTGGTTCTCGTGCCGACTTTATCGATATGGTCAACACGTGTCGTGAAGCTGGTGTGAAAATCTATGT
CGACGCCGTGATTAATCACATGACCGGGACCGGTAGTGCTGGAGCTGGCCCTGGTTCCGCTGGCTCATCC
TATTCAAAATATGACTATCCGGGCATCTATCAGTCACAGGACTTCAACGATTGCCGTCGTGATATTACCA
ACTGGAATGACAAATGGGAGGTCCAACATTGTGAGCTGGTTGGCCTGGCAGATCTGAAAACCTCTAGCCC
GTATGTCCAGGATCGTATTGCCGCTTATCTGAACGAACTGATCGACCTGGGTGTTGCTGGATTTCGTATC
GACGCTGCTAAACACATTCCGGAAGGCGACCTGCAAGCAATTCTGTCTCGCCTGAAAAACGTTCATCCGG
CATGGGGTGGCGGTAAACCTTATATCTTTCAAGAAGTGATCGCCGATAGCACCATCTCTACAGGGTCCTA
TACACATCTGGGTAGCGTGACCGAGTTCCAGTATCACCGTGACATCAGTCATGCCTTTGCCAATGGGAAT
ATTGCCCATCTGACTGGACTGGGTAGTGGTCTGACACCTTCGGACAAAGCAGTGGTTTTTGTGGTTAACC
ATGACACTCAGCGCTATGAACCGATTCTGACTCATACCGACGGTGCTCGTTATGATCTGGCCCAGAAATT
CATGCTGGCTCACCCGTATGGTACACCGAAAGTCATGTCCTCGTATACCTGGTCAGGGGATGACAAAGCT
GGTCCGCCTATGCATTCTGACGGTACTACTCGTCCTACAGACTGTTCTGCCGATCGCTGGCTGTGTGAAC
ATCGTGCCGTTGCTGGTATGGTTGGCTTCCATAATGCCGTGGCCGGACAGGGAATTGGTAGCGCCGTTAC
CGATGGAAACGGTCGTCTGGCTTTTGCTCGTGGATCCGCCGGTTATGCTGCCTTTAATGCCACGAATACC
GCTTGGACTCGTACCTTTACCACCTCTCTGCCTGATGGCGTTTATTGTGATGTGGCGAATGGCACCTTTG
TTGATGGCGTCTGTGATGGTCCGTCTTATCAGGTTAGTGGGGGCAAATTCACAGCAACTGTTCCGGCAAA
TGGTGCCGTAGCACTGCATGTCGAAGCACCTGGTTCTTGTGGCCCTGATGGTTGTGGCACACCTCCTGGT
GGAGGGGACGACTGTACTACTGTTACAGCCCGCTTTCACGCCACAGTAACAACATGGTATGGCCAAGAAG
TTGCCGTTGTAGGCTCTATCCCTGAACTGGGATCATGGCAACCTGCCCAAGGCGTTCGTCTGCGTACAGA
TTCTGGCACTTATCCGGTGTGGTCTGGTGCCGTTGACCTGCCTGCTGGTGTTGGCTTTGAGTATAAATAT
GTAAAACTGAATCCGGACGGTACTGTTGAGTGGGAGCAGGGTGGGAACCGTATCGCTACTGTCGATGATA
GCGGAGGCGGTTGTTCTCAGAACTTTTATGACTCCTGGCGCTAATAAAAGCTT

Stop *Hind* III

Supplementary Figure S2: Nucleotide sequence of TFA engineered for *E. coli* expression

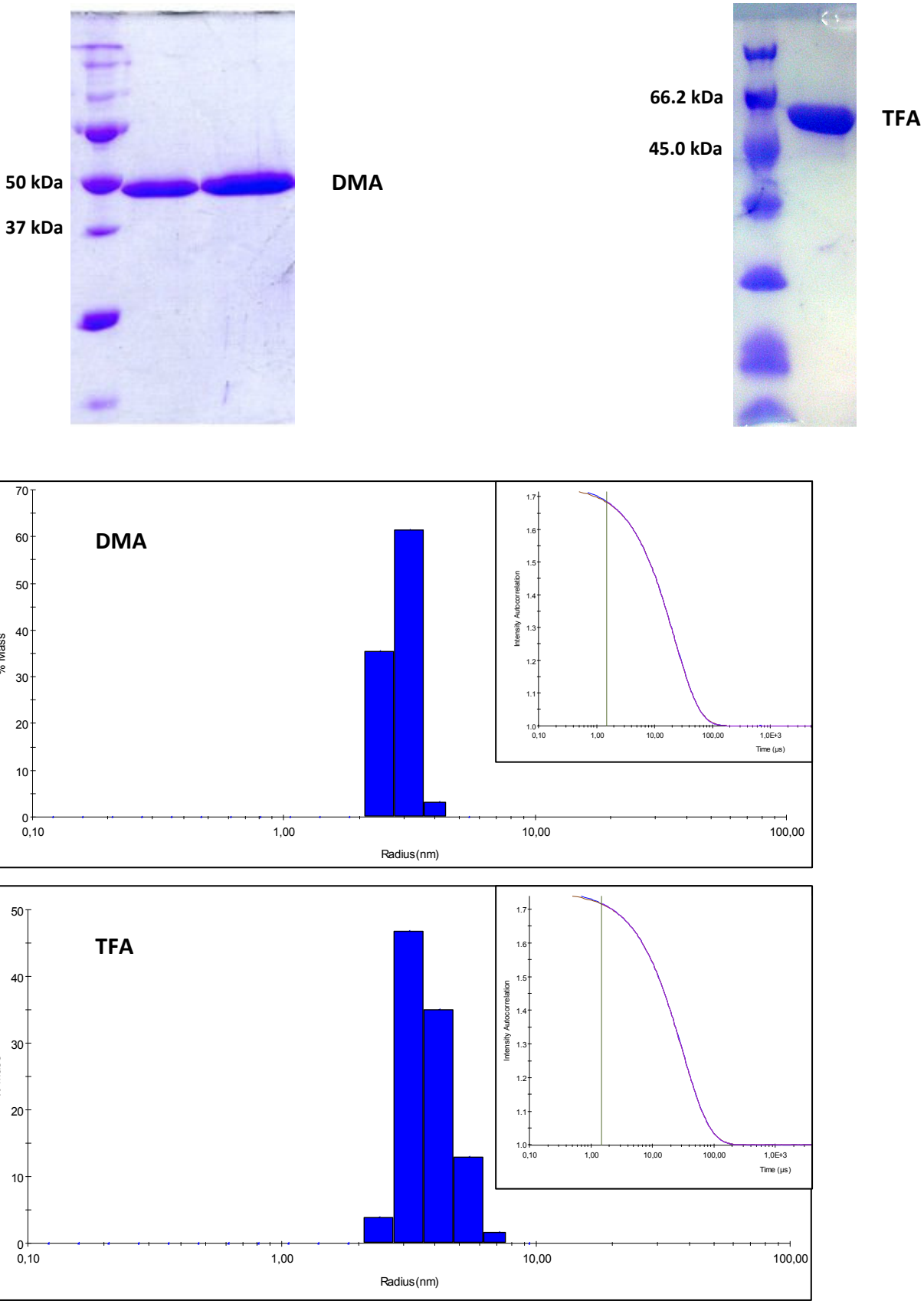

Supplementary Figure S3: Homogeneity of the newly purified α-amylases. Upper panel: SDS-PAGE of DMA and TFA samples. **Lower panels:** hydrodynamic radius distribution and autocorrelation function (inset) from dynamic light scattering. Mean radius and polydispersity were 3.1 nm and 14% for DMA, and 3.8 nm and 20% for TFA.

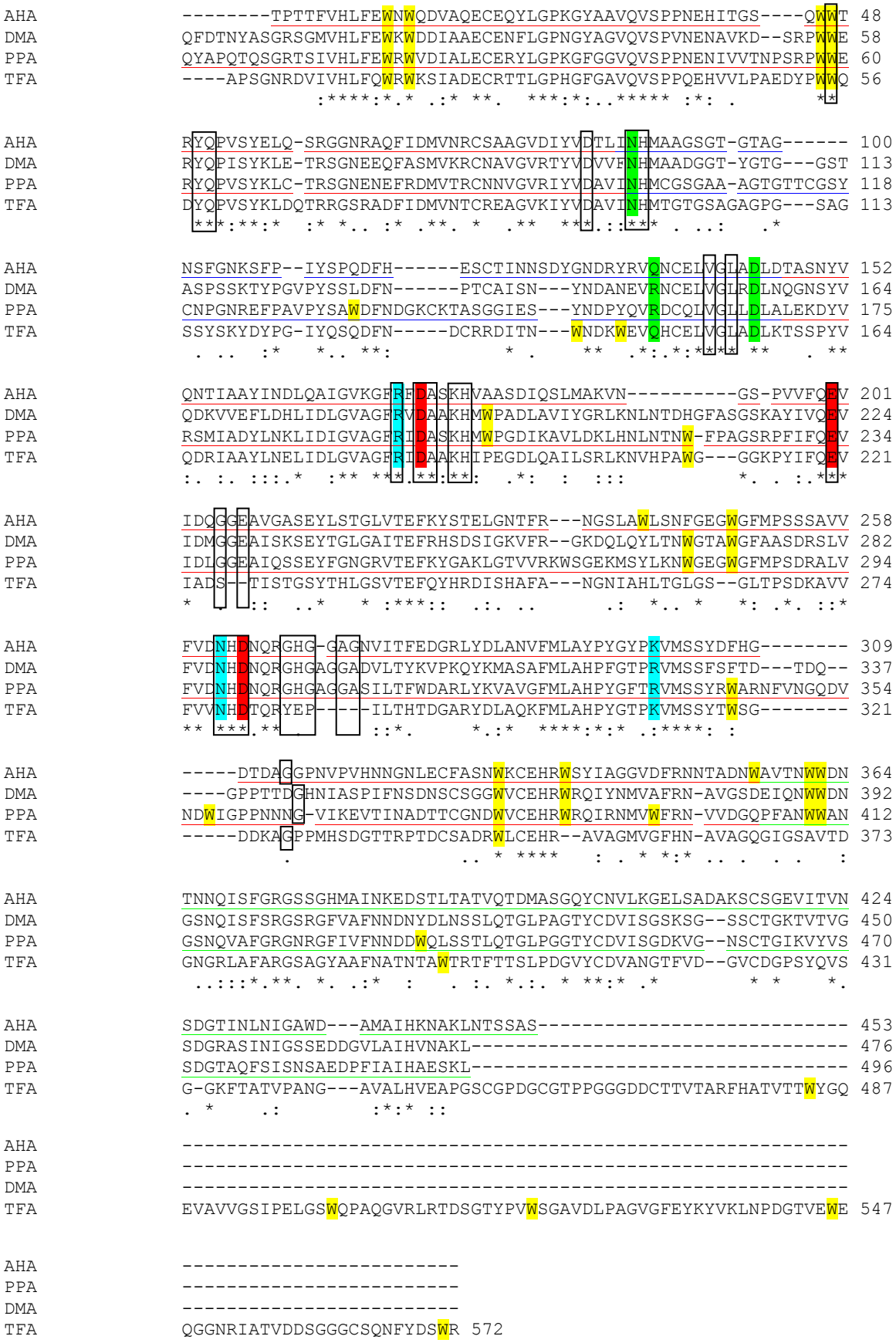

Supplementary Figure S4: Multiple sequence alignment by CLUSTALW2. Structural domains in AHA and PPA are underlined (domains A, B and C). Active site residues are boxed. Some important residues are indicated: catalytic residues (red), chloride binding site (blue), calcium binding site (green), and tryptophan residues (yellow).

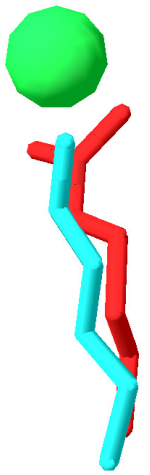

Supplementary Figure S5: Coordination of the chloride ion in α-amylases. Superimposition of the crystal structures of AHA (1AQH) and of PPA (1PPI) showing the main ligand of the chloride ion (green sphere). In AHA (blue) lysine provides monodentate coordination whereas in PPA (red) arginine provides bidentate coordination (adapted from [30])

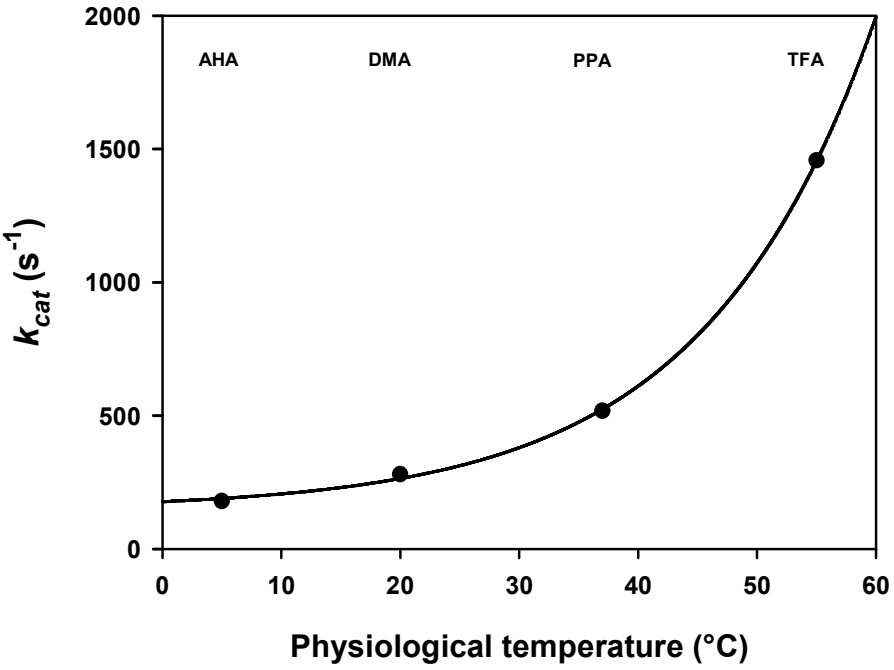

Supplementary Figure S6: Graphical representation of α-amylase activity at their environmental/physiological temperatures. Data from Table 3 in the main text. The solid line represents the fit of the data on an exponential growth.

Supplementary Table S1

Thermodynamic parameters of activation at relevant environmental/physiological temperatures

	T (°C)	k_{cat} (s^{-1})	E_a (kcal mol^{-1})	$\Delta G^{\#}$ (kcal mol^{-1})	$\Delta H^{\#}$ (kcal mol^{-1})	$T\Delta S^{\#}$ (kcal mol^{-1})
AHA	5	179	8.9	13.4	8.3	-5.0
DMA	20	280	10.9	13.9	10.3	-3.5
PPA	37	518	12.0	14.3	11.4	-2.9
TFA	55	1457	22.9	14.5	22.2	7.7